Observation of W IV W VII line emissions in wavelength range of 495 1475 A in the large helical device

Observation of W IV - W VII line emissions in wavelength range of 495-1475 Å in the Large Helical Device

Tetsutarou OISHI[1,2], Shigeru MORITA[1,2], Xianli HUANG[2], Hongming ZHANG[2],

Motoshi GOTO[1,2] and the LHD Experiment Group[1]

[1]*National Institute for Fusion Science,322-6 Oroshi-cho, Toki 509-5292, Gifu, Japan*

[2]*Department of Fusion Science, Graduate University for Advanced Studies, 322-6 Oroshi-cho, Toki 509-5292, Gifu, Japan*

Abstract

Vacuum ultraviolet (VUV) spectra of line emissions from tungsten ions at lower ionization stages have been measured in the Large Helical Device (LHD) using a high-resolution 3m normal incidence spectrometer in the wavelength range of 495 to 1475 Å. Tungsten was introduced in the LHD plasma by injecting a coaxial tungsten impurity pellet. Many tungsten lines of W IV - W VII were successfully observed in low-temperature plasmas just after the tungsten pellet injection. It is found that some W VI lines are emitted with extremely high intensity and entirely isolated from other intrinsic impurity lines, in particular, W VI at 605.926 Å (5d-6p), 639.683 Å (5d-6p), 677.722 Å (5d-6p), 1168.151 Å (6s-6p) and 1467.959 Å (6s-6p). The result strongly suggests that those lines may be useful for the spectroscopic study in ITER and other magnetic fusion devices with tungsten materials as the plasma facing component. The ion temperature was also measured from Doppler broadening of W V and W VI lines. The result indicates that the measured ion temperature is clearly higher than the ionization energy of such ions. The reason is discussed with regarding to the pellet injection.

1.Introduction

Tungsten is regarded as a possible candidate material for the plasma facing component (PFC) in divertor region of ITER and future fusion reactors because of its high melting point, low sputtering yield, and low tritium retention [1-3]. One of the major concerns regarding the tungsten PFC is that the tungsten ion causes a large radiation loss due to its large atomic number of Z = 74 when the plasma is contaminated by the tungsten impurity. At present, therefore, study of tungsten behaviors in fusion devices is crucially important. At the initial stage of the tungsten transport process in fusion devices with tungsten PFCs, firstly, neutral tungsten atoms sputtered and released from the divertor plates are ionized in the divertor region and start to move upstream toward X-points along magnetic field lines. The singly ionized tungsten ion is a tungsten impurity influx to the scrape-off layer of tokamaks. On the other hand, a line emission from the tungsten neutrals has been measured at the wavelength of λ = 4009 Å, using visible spectroscopies as an indicator of the sputtering yield [4,5]. Once the tungsten ion enters the main plasma passing through the scrape-off layer, it is ionized to higher ionization stages in the core region of high-temperature plasmas. A large number of tungsten line emissions from highly ionized tungsten ions have been measured in the past in the wavelength ranges of extreme ultraviolet (EUV) and soft X-ray (SX). For example, the line emissions at λ = 61 Å from W^{44+} ions and 62 Å from W^{45+} ions have been observed in the plasma center and utilized to study the impurity accumulation phenomena [6,7]. An imaging diagnostic of SX radiation from highly-ionized tungsten ions has also been developed to measure the two-dimensional distribution of tungsten emissions on a poloidal cross section [8,9].

On the other hand, tungsten ions at lower ionization stages existing in edge and divertor plasmas including the scrape-off layer have rarely been observed until now in the present fusion devices, while the line emission from low-ionized tungsten is necessary for accurate evaluation of tungsten influx and understanding of the tungsten transport in the

scrape-off layer or edge plasma. The line emissions from tungsten ions in such low charge states have only been measured in several basic plasma experiments based on vacuum ultraviolet (VUV) spectroscopy [12,13]. Figure 1 shows ionization energy of tungsten ions, E_i, as a function of charge state, q^+ [10]. In fusion plasmas the impurity ion is basically located in a radial position where the electron temperature, T_e, is equal to E_i. Although accurate determination of the radial position where the impurity ion is located requires further discussion on impurity and plasma transport, we can obtain a rough guideline of the impurity location by assuming $T_e = E_i$. According to a numerical simulation by the ITER Physics Expert Group on Divertor, the value of T_e in ITER divertor plasmas ranges below 150 eV [11]. A grey-striped region indicates the electron temperature range for typical ITER divertor plasmas. From the figure, observation of W^{8+} (E_i = 160.2 eV), W^{7+} (E_i = 141.2 eV), and tungsten ions in further low-charge states are expected in the divertor plasma. Thus, application of the VUV spectroscopy to high temperature plasma experiments is very important for identification of line emissions from tungsten ions in lower charge states which leads to the tungsten transport study in edge plasmas and also the quantitative evaluation of tungsten influx in fusion plasmas in addition to the enhancement of spectroscopic database on tungsten line emissions.

Based on the background mentioned above, VUV spectra from low-ionized tungsten are measured in the Large Helical Device (LHD) for the contribution to the tungsten transport study in edge plasmas of ITER and other tungsten-divertor fusion devices and for the expansion of experimental database of tungsten line emissions.

2. Tungsten pellet injection experiment in LHD

High-density and high-temperature plasmas in LHD are produced and maintained by negative-ion-source-based neutral beam injection (n-NBI) with high beam energy of 180

keV and high port-through power of 18 MW in the absence of toroidal plasma current [14]. Typical electron temperature range at the core plasma of NBI discharges in the standard configuration (major/minor radii of 3.6/0.64 m, plasma volume of 30 m^3 and toroidal magnetic field of 3 T) is indicated by the gray region in Fig.1. The electron temperature at the plasma center and the plasma edge defined by the last closed flux surface (LCFS) ranges in $2 \leq T_e \leq 3$ keV and $0.15 \leq T_e \leq 0.5$ keV, respectively, depending on the electron density.

In order to observe the tungsten emission a tungsten impurity pellet accelerated by pressurized He gas of 10-20 atm is injected in the LHD plasma with speed of ~200 m/s. The tungsten impurity pellet has a coaxial structure of a thin tungsten wire inserted into a polyethylene or carbon cylindrical tube [15,16]. Since the tungsten wire with sizes of 0.6 mm in length and 0.15 mm in diameter is used in the present experiment, approximately 7×10^{16} tungsten atoms are deposited in the plasma at single pellet injection. In the present study, the VUV spectroscopy was attempted for hydrogen discharges with magnetic axis position of R_{ax}, = 3.60 m at toroidal magnetic field of B_t, = -2.75 T. Here, the minus sign of B_t means inverse direction, i.e., counter-clockwise direction. Figure 2 shows a typical waveform in experiments with the tungsten pellet injection. The discharge initiated by the electron cyclotron heating is grown by three n-NBI beams with total port-through power of 10 MW and maintained for 5 s as shown in Fig. 2(a). Figures 2 (b), (c), (d) and (e) show the central electron temperature, T_{e0}, the central electron density, n_{e0}, the electron kinetic energy, W_{pe}, and the total radiation power, P_{rad}, respectively. After the tungsten pellet injection at 4.3 s, T_{e0} and W_{pe} quickly decrease, while n_{e0} increases. It has been confirmed experimentally that the increase in n_e is caused by ablation of tungsten in the pellet dominantly and increase in n_e by carbon ablation in the pellet is small [15]. P_{rad} once increases significantly and turns to decrease at 4.35 s. After T_{e0} reaches the minimum value around 0.5 keV, T_{e0} starts to recover. During the T_{e0} recovery phase, P_{rad} continues to

decrease and line emissions from tungsten ions appear in the order from lower to higher ionization stages.

Temporal evolutions of electron temperature and density profiles in the same discharge as Fig. 2 are plotted in Figs. 3(a) and (c) and Figs. 3(b) and (d), respectively. The profiles at t = 4.266 s (open circles) and 4.4 s (solid circles) indicates ones just before and after the tungsten pellet injection, respectively. When the pellet is injected, the edge T_e rapidly drops and the edge n_e quickly increases because the pellet is evaporated in the plasma edge, as shown in Figs. 3(a) and (b). Figure 3(c) and (d) show increases of core T_e and n_e, respectively, in a phase in which T_e recovers (4.8-5.4 s).

The large variation of T_e after the tungsten pellet injection as shown in Fig. 2 can provide us an excellent opportunity to observe tungsten line emissions in various kinds of charge states as a function of discharge time. In the previous studies in LHD, EUV spectroscopy has been extensively carried out by observing tungsten line emissions at the temperature recovery phase. Unresolved transition array (UTA) from tungsten ions in ionization stages of W^{24+} to W^{33+} is clearly observed in the wavelength range around 50 Å in the time sequence when T_e recovers from 0.13 keV to 1.7 keV. The line emission from W^{44+} ions at 61 Å and its radial profile also have been successfully observed in the temperature recovery phase at $2.3 \leq T_e \leq 3.2$ keV [17]. In the present study, the VUV spectroscopy is attempted in the temperature reduction phase at which low-ionized tungsten ions are expected to exist in the plasma core. Therefore, it strongly suggests that VUV line emissions from such ions can be measured with sufficient intensity.

3. VUV spectra of W IV-W VII in wavelength range of 495-1475Å

A 3m normal incidence VUV spectrometer (McPherson model 2253) working in the wavelength range of 300-3200 Å is installed on an outboard midplane diagnostic port with

the impurity pellet injector as shown in Fig. 4(a) [18]. A back-illuminated CCD detector (Andor model DO435-BN: 1024 × 1024 pixels) is used for measuring a focal image of VUV line emissions at the exit slit of the spectrometer. A high wavelength dispersion of 0.037 Å/pixel enables Doppler profile measurement of the impurity lines basically over the whole wavelength range. The viewing angle covers an entire vertical region of the elliptical LHD plasma at horizontally-elongated poloidal plasma cross section to measure the top-to-bottom vertical profile as shown in Fig. 4(b). In this study, the wavelength spectrum is simply measured instead of the vertical profile diagnostic by fully opening the spatial-resolution slit for detailed observations of tungsten line emissions. For the purpose the CCD is operated in "full-binning" mode with time resolution of 50 ms. The CCD then works as a linear detector by summing up all 1024 vertical pixels. The wavelength interval which can be measured in a single discharge is about 37 Å, and does not depend significantly on the wavelength range to be measured. Since the wavelength interval is quite narrow due to the high dispersion of the spectrometer, the measurement of tungsten line emissions is carried out by changing the central wavelength for each shot in the wavelength range of 495-1475 Å. Therefore, at least 28 successful discharges were necessary for observation over the whole wavelength range.

Many VUV line emissions from low-ionized tungsten, i.e., W IV, W V, W VI and W VII, were successfully observed at the time frame just after the tungsten pellet injection, in particular, the time frame of 4.30-4.35 s in Fig. 2. The observed tungsten VUV spectra are displayed in Fig.5. It should be noticed here that the plasma parameters rapidly change during the signal integration time of 50 ms. The observed spectrum therefore includes information at temporally changing plasma parameters. In addition, the discharge behavior after the tungsten pellet injection has some variation for each shot. The discharge condition during observation of the tungsten spectrum is not then identical in a very strict sense. In order to examine an effect of the temporal change of plasma parameters and conditional variation among discharges the tungsten spectrum was observed in several discharges with

tungsten pellet by fixing the wavelength. However, the observed spectra did not show any large difference in the spectral intensity and structure. This indicates the tungsten spectra observed in the present study can be a typical dataset from low-temperature fusion plasmas. Each line in Fig.5 is carefully identified using the NIST atomic spectra database [10]. The line emission in each ionization stage of W IV, W V, W VI and W VII are drawn in purple, blue, green and orange solid lines and denoted with arrows in the same colors, while line emissions from intrinsically existing impurity ions and tungsten lines blended with other lines are drawn in black dashed lines and denoted with black dashed arrows in Fig. 5. The wavelength scale in abscissa of Fig.5 is determined by linear interpolation and extrapolation based on the wavelengths of intrinsic or extrinsic impurity ions (H, He, B, C, N, O and Fe) which have been already known with high accuracy. A brief description of observed lines is summarized in the following.

3.1 W IV

The W IV lines appear at longer wavelengths of in the VUV range which are mainly seen in Figs. 5(d)-(g). The spectral identification is listed in Table 1 with relative spectral intensity. λ_{NIST} and λ_{obs} are the wavelengths of line emissions registered in Ref. [10] and observed by our VUV spectroscopy, respectively. Discrepancy between λ_{NIST} and λ_{obs} is much smaller than 0.1 Å for all identified lines, which indicates a high accuracy of the line identification. The spectral intensity is evaluated as count rate (counts/50ms) at the peak channel of line emissions by subtracting the background level. The intensity of W IV lines is relatively weak and most of the lines are blended with other lines. In Table 1 the blended line is denoted as 'b' in the column of relative intensity. Since the ionization energy of W^{3+} ions is very small, i.e., 38.2 eV, the W IV emission is located in outer region of the LHD plasma even if the electron temperature largely drops after the tungsten pellet injection. This indicates a small emission volume along the viewing chord, which leads to weaker

intensity. In addition, there are many transitions in the W IV isoelectronic sequence reflecting its complex electronic structure, i.e., three 5d electrons in the outer shell. This suggests that the intensity of single transition is relatively weaker. These may be a possible reason why the intensity of W IV is weak.

3.2 W V

The W V lines are also identified in a wide wavelength range of 715-1475 Å as well as in the case of W IV. The result is shown in Figs. 5(b)-(g) and the identification is summarized in Table 2. The line intensity of W V is generally stronger than that of W IV. In the W V isoelectronic sequence we can select typical isolated lines with substantial intensity as follows; W V lines at 797.649 Å, 810.228 Å, 811.459 Å, 814.648 Å, 817.489 Å, 821.190 Å, 842.724 Å, 847.744 Å, 867.637 Å, 1305.614 Å and 1311.472 Å.

3.3 W VI

In the VUV line emission from low-ionized tungsten ions the W VI line gives the strongest intensity because the electronic structure in the W VI isoelectronic sequence is relatively simple. As the W^{5+} ion only has single 5d electron in the outer shell, the number of transitions is very limited. Therefore, the intensity of each transition becomes stronger. In particular, five W VI transitions at 605.926 Å (5d-6p), 639.683 Å (5d-6p), 677.722 Å (5d-6p), 1168.151Å (6s-6p) and 1467.959 Å (6s-6p) have very strong intensity as listed in Table 3. These lines are useful for the spectroscopic study because they are entirely isolated from other impurity lines in addition to the sufficient intensity.

It is worth stating that one may suspect an effect of the superposition of the WVI 677.722 Å line and the BIII 677.142 Å line because the BIII line is one of strong lines among boron lines, even though the BIII line is not identified in the present case shown in Fig. 5(b). Due to a high wavelength dispersion of 0.037 Å/pixel, difference of wavelengths of these two

lines 0.58 Å is about 16 pixels. It is large enough to distinguish these two lines in the spectrum when BIII 677.142 Å emission becomes significant. We also measured WVI lines using poor-resolution VUV spectrometers with 0.85 Å/pixel, which cannot distinguish between WVI 677.722 Å and BIII 677.142 Å. Then temporal evolutions of line emission intensities of WVI 639.683 Å and WVI 677.722 Å are proportional to each other [19]. It suggests that superposition of the WVI 677.722 Å and BIII 677.142 Å is negligible.

3.4 W VII

The W VII lines are dominated in shorter wavelength range of 495-600 Å as seen in Fig. 5(a). Second order emissions of those lines can also be observed in the wavelength range of 900-1200 Å (see Figs.5 (d) and (e)). However, these lines are not sufficiently adequate for the spectroscopic study of tungsten because the intensity is relatively weak and most of the lines are blended with other lines. The throughput of the present 3m normal incidence spectrometer system gradually decreases below 1000 Å [20], while it is roughly constant above 1000Å. The absolute intensity calibration has not been performed yet. However, the spectral intensity from intrinsic impurities of carbon and oxygen is still strong as seen in Fig. 5(a). When the line ratio is taken into account for carbon and oxygen lines, the throughput reduction at 500-600 Å is at least much smaller than order of magnitude. Therefore, the relatively weak intensity of W VII is not mainly caused by the reduction of the spectrometer throughput.

3.5 W V and W VI lines useful for tungsten diagnostics

The W VI and W V lines which seem to be useful for tungsten diagnostics are listed in Table 5. Measurement of Doppler profiles is attempted using such lines. Figures 6(a) and (b) show spectral profiles of W VI at 605.926 × 2 Å and W V at 1311.472 Å with Doppler broadening, respectively. The profile fitting to raw spectral data was very good due to the

sufficient signal intensity. The full width of half maximum (FWHM) in the Doppler broadening and resulting ion temperature, T_i, are determined with error bars. The result is also listed in Table 5. The spectral instrumental width of the spectrometer system is carefully examined using a low pressure mercury lamp (HAMAMATSU L937-02) and VUV lines from neutral mercury particles with extremely low T_i. It is finally determined to be 0.206 ± 0.06 Å in FWHM of which the value is basically independent of the wavelength. The T_i is thus calculated by taking into account the instrumental width. However, the error bar of T_i listed in Table 5 is still large except for a few tungsten lines at 2nd order light and longer wavelength, e.g. W VI at 605.926 × 2 Å and W V at 1311.472 Å. This means that the error bar is mainly caused by a lack of spectral resolution of the spectrometer system but not by a lack of signal intensity. It is difficult to discuss difference among T_i from different transitions or charge states using present data quality. However, we can expect to observe higher order emissions of the lines listed in this table within the observable wavelength range, $\lambda < 3200$ Å, because the observed intensity of tungsten lines are relatively strong. If we can find higher order emissions with broader Doppler width in future studies, it will lead to improve the signal to noise ratio for the T_i measurements. At present, available discussion is limited to an overall tendency that the measured T_i seems to be higher than the ionization energy of W^{4+} and W^{5+} which is 51.6 eV and 64.8 eV, respectively. In LHD the electron temperature where the impurity ion exists, T_{eZ}, was compared with the ionization energy [21]. In the previous study the T_{eZ} is almost equal to the ionization energy for the impurity ion existing at plasma edge, while the T_{eZ} is considerably smaller than the ionization energy for the impurity staying at the plasma core. If this condition can be applied to low-ionized tungsten ions, the measured T_i should be equal to the ionization energy. The ionization time of W^{4+} or W^{5+} ions is smaller than 1ms and much smaller than the data acquisition time (= 50 ms). The tungsten ions are then already in the ionization equilibrium. The T_e rapidly decreases due to the large ionization and radiation losses after the tungsten

pellet injection, while the bulk ion loses the energy through collision with electrons. However, the energy exchange time between ion and electron is considerably long in the discharge shown in Fig.2, e.g., 50 ms [22]. Therefore, the T_i seems to be higher than the T_e as a transient effect just after the tungsten pellet injection. This will be a possible explanation of why the T_i of the tungsten ions is higher than the ionization energy.

4. Summary

VUV spectroscopy using a high-resolution 3 m normal incidence spectrometer has been applied to measure VUV lines from tungsten ions at lower ionization stages in wavelength range of 495-1475 Å in LHD. The tungsten is externally introduced in the LHD plasma by injecting a coaxial tungsten impurity pellet. Many tungsten lines of W IV - W VII were successfully observed just after the tungsten pellet injection. It is found that five W VI lines at 605.926 Å, 639.683 Å, 677.722 Å, 1168.151 Å and 1467.959 Å have the highest intensity and are entirely isolated from other intrinsic impurity lines. The result strongly suggests that those lines will be useful for the spectroscopic study in ITER and other tungsten-divertor devices. The ion temperature was measured from Doppler broadening of W V and W VI lines. The measured ion temperatures were higher than the ionization energy, suggesting a transient effect after the pellet injection.

Acknowledgements

The authors thank all the members of the LHD Experiment Group for their cooperation with the LHD operation. This work is partially conducted under the LHD project financial support (NIFS14ULPP010). This work was also supported by Grant-in-Aid for Young Scientists (B) 26800282 and partially supported by the JSPS-NRF-NSFC A3

Foresight Program in the Field of Plasma Physics (NSFC: No.11261140328, NRF: No.2012K2A2A6000443).

References

[1] D. W. Ignat *et al.*, Nucl. Fusion **39**, 2137 (1999).

[2] R. Neu *et al.*, Nucl. Fusion **45**, 209 (2005).

[3] J. Roth *et al.*, Plasma Phys. Control. Fusion **50**, 103001 (2008).

[4] R. Dax *et al.*, J. Nucl. Mater. **390-391**, 858 (2009).

[5] T. Nakano *et al.*, Nucl. Fusion **49**, 115024 (2009).

[6] T. Pütterich *et al.*, Plasma Phys. Control. Fusion **50**, 085016 (2008).

[7] T. Nakano, The JT-60 Team, J. Nucl. Mater. **415**, S327 (2011).

[8] C. Angioni *et al.*, Nucl. Fusion **54**, 083028 (2014).

[9] F. J. Casson *et al.*, Plasma Phys. Control. Fusion **57**, 014031 (2015).

[10] A. Kramida *et al.*, (2014). NIST Atomic Spectra Database (ver. 5.2), [Online]. Available: http://physics.nist.gov/asd [2015, August 27]. National Institute of Standards and Technology, Gaithersburg, MD.

[11] ITER Physics Expert Group on Divertor, Nucl. Fusion **39**, 2391 (1999).

[12] R. Radtke *et al.*, Atomic and Plasma-Material Interaction Data for Fusion **13**, 45 (2007), IAEA Safety Related Publications.

[13] J. Clementson *et al.*, J. Phys. B: At. Mol. Opt. Phys. **43**, 144009 (2010).

[14] H. Yamada for the LHD Experiment Group, Nucl. Fusion **51**, 094021 (2011).

[15] X. L. Huang *et al.*, Rev. Sci. Instrum. **85**, 11E818 (2014).

[16] H. Nozato *et al.*, Rev. Sci. Instrum. **74**, 2032 (2003).

[17] S. Morita *et al.*, AIP conference proceedings **1545**, 143 (2013), Proceedings of ICAMDATA-2012, Gaithersburg, 30 Sept.–4 Oct. 2012.

[18] T. Oishi *et al.*, Appl. Opt. **53**, 6900 (2014).

[19] T. Oishi *et al.*, Plasma Fus. Res. **10**, 3402031 (2015).

[20] Z. Y. Cui *et al.*, Rev. Sci. Instrum. **81**, 043503 (2010).

[21] C. F. Dong *et al.*, Plasma Sci. Technol. **13**, 140 (2011).

[22] S. Morita *et al.*, Nucl. Fusion **43**, 899 (2003).

Table 1 Wavelength list of VUV lines from W IV ($5s^2 5p^6 5d^3$). Symbol 'b' in relative intensity means the line is blended with other lines.

λ_{NIST} (Å)	λ_{obs} (Å)	λ_{NIST} - λ_{obs} (Å)	Relative intensity (counts /50ms)	λ_{NIST} (Å)	λ_{obs} (Å)	λ_{NIST} - λ_{obs} (Å)	Relative intensity (counts /50ms)
876.748			b	1161.365			b
876.898			b	1161.426			b
889.777	889.734	0.043	142	1167.164			b
935.856	935.807	0.049	60	1172.471			b
968.837	968.914	-0.077	73	1175.621			b
987.065	987.08	-0.015	102	1186.174	1186.177	-0.003	140
995.867	995.868	-0.001	52	1193.451			b
1003.859			b	1202.899			b
1006.670			b	1208.885			b
1036.571			b	1225.692	1225.651	0.041	67
1041.591	1041.590	0.001	135	1242.856			b
1046.047	1046.060	-0.013	75	1247.307			b
1048.245	1048.209	0.036	76	1247.368			b
1049.204			b	1249.230			b
1051.503			b	1259.482			b
1063.288	1063.261	0.027	95	1293.094			b
1068.248			b	1301.215			b
1068.250			b	1309.520			b
1068.630			b	1312.280			b
1072.963	1072.955	0.008	146	1332.102			b
1074.748			b	1334.539			b
1088.027	1088.025	0.002	76	1334.579			b
1093.261			b	1338.699			b
1097.653	1097.672	-0.019	72	1340.640	1340.635	0.005	134
1098.240			b	1343.084			b
1099.049			b	1353.548	1353.543	0.005	168
1102.938			b	1354.489	1354.492	-0.003	254
1106.154	1106.158	-0.004	48	1370.023			b
1112.433	1112.432	0.001	188	1372.005			b
1113.935	1113.932	0.003	142	1379.588	1379.558	0.03	243
1119.718	1119.705	0.013	97	1390.623			b
1135.148	1135.157	-0.009	70	1404.040			b
1136.937	1137.015	-0.078	49	1406.866			b
1140.273			b	1452.248	1452.285	-0.037	128
1140.337			b	1455.504			b
1152.570			b	1464.327			b
1153.898			b	1470.239			b
1161.360			b				

Table 2　Wavelength list of VUV lines from W V ($5s^25p^65d^2$). Symbol 'b' in relative intensity means the line is blended with other lines.

λ_{NIST} (Å)	λ_{obs} (Å)	λ_{NIST} - λ_{obs} (Å)	Relative intensity (counts /50ms)	λ_{NIST} (Å)	λ_{obs} (Å)	λ_{NIST} - λ_{obs} (Å)	Relative intensity (counts /50ms)
716.727	716.721	0.006	139	435.023×2	870.07	-0.024	164
723.876	723.877	-0.001	190	873.042	873.032	0.01	238
725.623	725.617	0.006	84	875.102	875.098	0.004	121
726.167	726.168	-0.001	313	441.073×2	882.144	0.002	66
730.525	730.533	-0.008	50	887.575	887.575	0	363
731.726	731.729	-0.003	207	448.510×2	897.047	-0.027	89
733.561	733.59	-0.029	90	453.849×2	907.709	-0.011	59
738.451	738.448	0.003	150	455.416×2	910.812	0.02	73
744.887	744.892	-0.005	401	913.350	913.344	0.006	220
752.845	752.84	0.005	89	457.732×2	915.474	-0.01	58
757.424	757.442	-0.018	107	933.413	933.412	0.001	113
760.743			b	942.951	942.969	-0.018	77
775.211	775.207	0.004	166	953.095	953.09	0.005	135
780.888	780.872	0.016	175	1189.140			b
785.898			b	1262.704	1262.697	0.007	184
786.254	786.252	0.002	739	1264.060	1264.055	0.005	183
797.056	797.05	0.006	189	1286.468			b
797.649	797.647	0.002	1069	1291.759			b
800.829	800.825	0.004	111	1305.614	1305.613	0.001	697
809.569	809.594	-0.025	80	1311.472	1311.473	-0.001	988
810.228	810.228	0	1236	1312.312			b
811.459	811.462	-0.003	1044	446.272×3			b
812.001			b	448.510×3			b
812.042			b	455.416×3			b
813.527	813.525	0.002	255	1367.344	1367.347	-0.003	455
814.648	814.654	-0.006	765	1373.453			b
817.489	817.492	-0.003	1007	1385.070			b
821.190	821.184	0.006	682	1399.948			b
823.868	823.863	0.005	188	468.928×3			b
829.448	829.442	0.006	117	1423.891			b
842.724	842.725	-0.001	993	479.035×3			b
847.744	847.749	-0.005	514	1445.421	1445.408	0.013	230
864.020	864.015	0.005	89	1455.570			b
867.637	867.631	0.006	502				

Table 3　Wavelength list of VUV lines from W VI ($5s^2 5p^6 5d$). Symbol 'b' in relative intensity means the line is blended with other lines.

λ_{NIST} (Å)	λ_{obs} (Å)	λ_{NIST} - λ_{obs} (Å)	Relative intensity (counts /50ms)	λ_{NIST} (Å)	λ_{obs} (Å)	λ_{NIST} - λ_{obs} (Å)	Relative intensity (counts /50ms)
605.926	605.929	-0.003	2096	1006.289	1006.295	-0.006	377
639.683	639.674	0.009	16535	1168.151	1168.147	0.004	3449
677.722	677.723	-0.001	13415	605.926×2	1211.860	-0.008	3081
394.134×2	788.265	0.003	388	639.683×2	1279.361	0.005	8417
876.106	876.112	-0.006	551	677.722×2	1355.442	0.002	7605
878.127	878.142	-0.015	163	1467.959	1467.954	0.005	1763
994.500			b				

Table 4 Wavelength list of VUV lines from W VII ($5s^25p^6$). Symbol 'b' in relative intensity means the line is blended with other lines.

λ_{NIST} (Å)	λ_{obs} (Å)	λ_{NIST} - λ_{obs} (Å)	Relative intensity (counts /50ms)	λ_{NIST} (Å)	λ_{obs} (Å)	λ_{NIST} - λ_{obs} (Å)	Relative intensity (counts /50ms)
495.078	495.119	-0.041	119	743.513	743.457	0.056	111
495.681	495.645	0.036	129	455.844×2	916.703	-0.015	135
496.424			b	483.912×2	967.834	-0.01	347
496.517			b	487.093×2	974.192	-0.006	214
497.337	497.327	0.01	371	496.424×2			b
498.655	498.669	-0.014	122	496.517×2			b
500.835	500.869	-0.034	120	331.534×3			b
501.438	501.466	-0.028	91	498.655×2	997.337	-0.027	83
501.993	501.998	-0.005	146	500.835×2			b
503.332			b	501.438×2	1002.887	-0.011	114
503.534			b	501.993×2			b
504.605	504.624	-0.019	120	503.332×2			b
510.490	510.51	-0.02	126	503.534×2	1007.077	-0.009	283
511.626			b	504.605×2	1009.224	-0.014	96
512.617	512.634	-0.017	486	510.490×2	1021.04	-0.06	102
513.549	513.512	0.037	47	511.254×2	1022.52	-0.012	123
516.582	516.595	-0.013	157	511.626×2			b
519.116	519.128	-0.012	97	512.617×2	1025.236	-0.002	458
520.321	520.325	-0.004	461	516.582×2	1033.188	-0.024	173
521.570	521.575	-0.005	124	518.275×2			b
523.250	523.259	-0.009	444	520.321×2	1040.643	-0.001	394
524.845	524.748	0.097	89	521.570×2	1043.188	-0.048	77
525.335	525.335	0	311	523.250×2	1046.494	0.006	340
527.620	527.617	0.003	325	1049.329			b
529.005	529.077	-0.072	52	525.335×2			b
530.954	530.929	0.025	240	527.620×2			b
533.630	533.605	0.025	437	530.954×2	1061.904	0.004	98
536.916	536.956	-0.04	296	533.630×2	1067.248	0.012	147
537.348	537.328	0.02	294	1070.577			b
540.495	540.431	0.064	86	537.348×2			b
542.954	543.008	-0.054	206	543.411×2			b
543.411	543.398	0.013	488	549.279×2			b
549.279	549.316	-0.037	210	551.448×2			b
557.973	557.937	0.036	70	596.999×2			b
560.322	560.332	-0.01	171	463.548×3			b
568.539	568.569	-0.03	91	464.020×3			b
596.999	597.012	-0.013	166	467.523×3			b

Table 5　List of VUV line emissions from W ions useful for spectroscopic measurement.

Charge state	Wavelength (Å)	Relative intensity (counts/50ms)	FWHM (Å)	Ion temperature (eV)
W VI	605.926	2096	0.207	51 ± 231
W VI	639.683	16535	0.211	167 ± 186
W VI	677.722	13415	0.214	228 ±166
W VI	1168.151	3449	0.219	121 ± 59
W VI	605.926 × 2	3081	0.221	137 ± 52
W VI	639.683 × 2	8417	0.219	102 ± 47
W VI	677.722 × 2	7605	0.231	182 ± 42
W VI	1467.959	1763	0.222	97 ± 37
W V	797.649	1069	0.213	139 ± 127
W V	810.228	1236	0.220	285 ± 126
W V	811.459	1044	0.214	155 ± 129
W V	817.489	1007	0.219	251 ± 129
W V	842.724	993	0.209	53 ± 120
W V	1311.472	988	0.232	208 ± 77

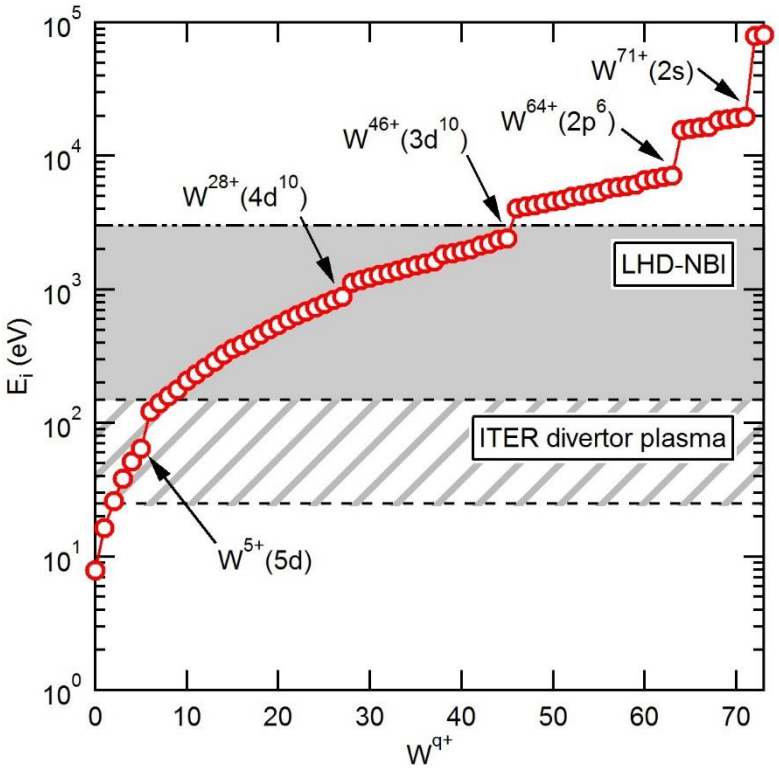

Figure 1　Ionization energy, E_i, of W ions as a function of charge state, $q+$. Grey-striped and gray-hatched regions indicate electron temperature range at $T_e = E_i$ for ITER divertor plasmas and LHD plasmas with NBI, respectively.

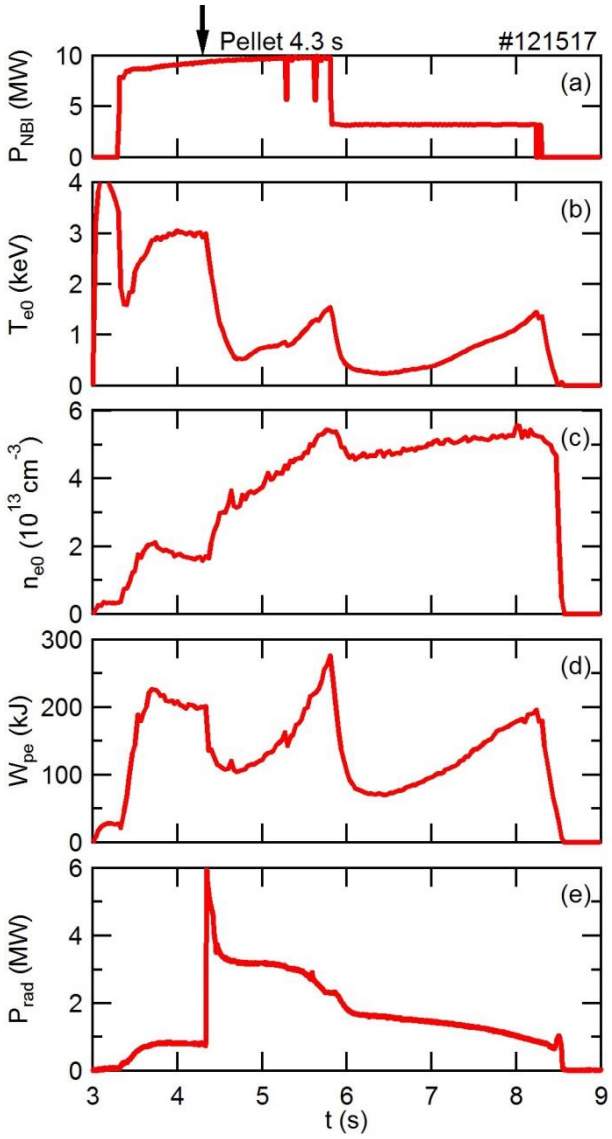

Figure 2　Typical waveform of W pellet injection experiment in LHD: (a) n-NBI power, (b) central electron temperature, (c) central electron density, (d) electron kinetic energy and (e) total radiation power.

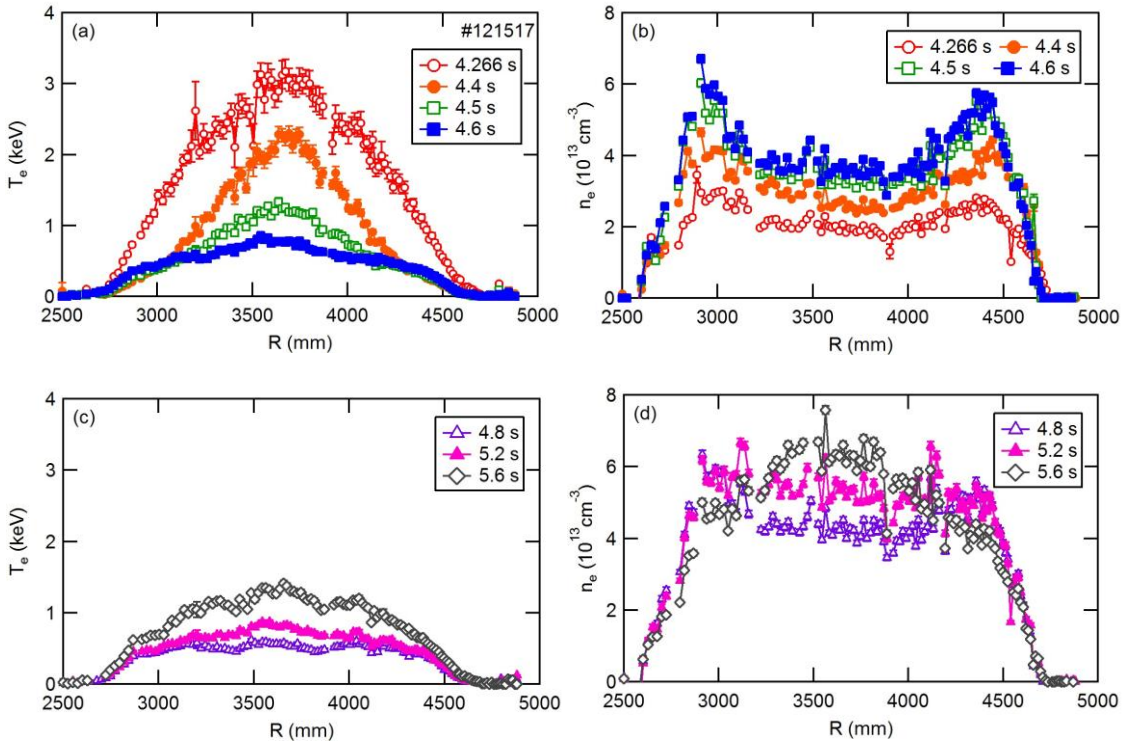

Figure 3 Temporal evolutions of radial profiles of electron temperature, T_e, and electron density, n_e: (a) T_e and (b) n_e profiles just before (4.266 s) and after (4.4-4.6 s) the pellet injection and (c) T_e and (d) n_e profiles in T_e recovery phase.

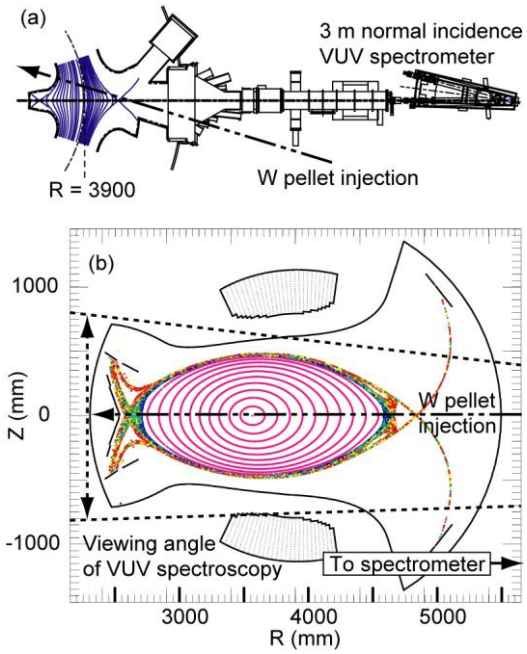

Figure 4　Schematic drawing of VUV spectroscopy in tungsten pellet injection experiments. (a) Top view of the instruments together with the optical axis of the VUV spectrometer and the injection direction of the tungsten pellet.　(b) Vertical viewing angle and the pellet injection direction on the poloidal cross section of the magnetic field in LHD.

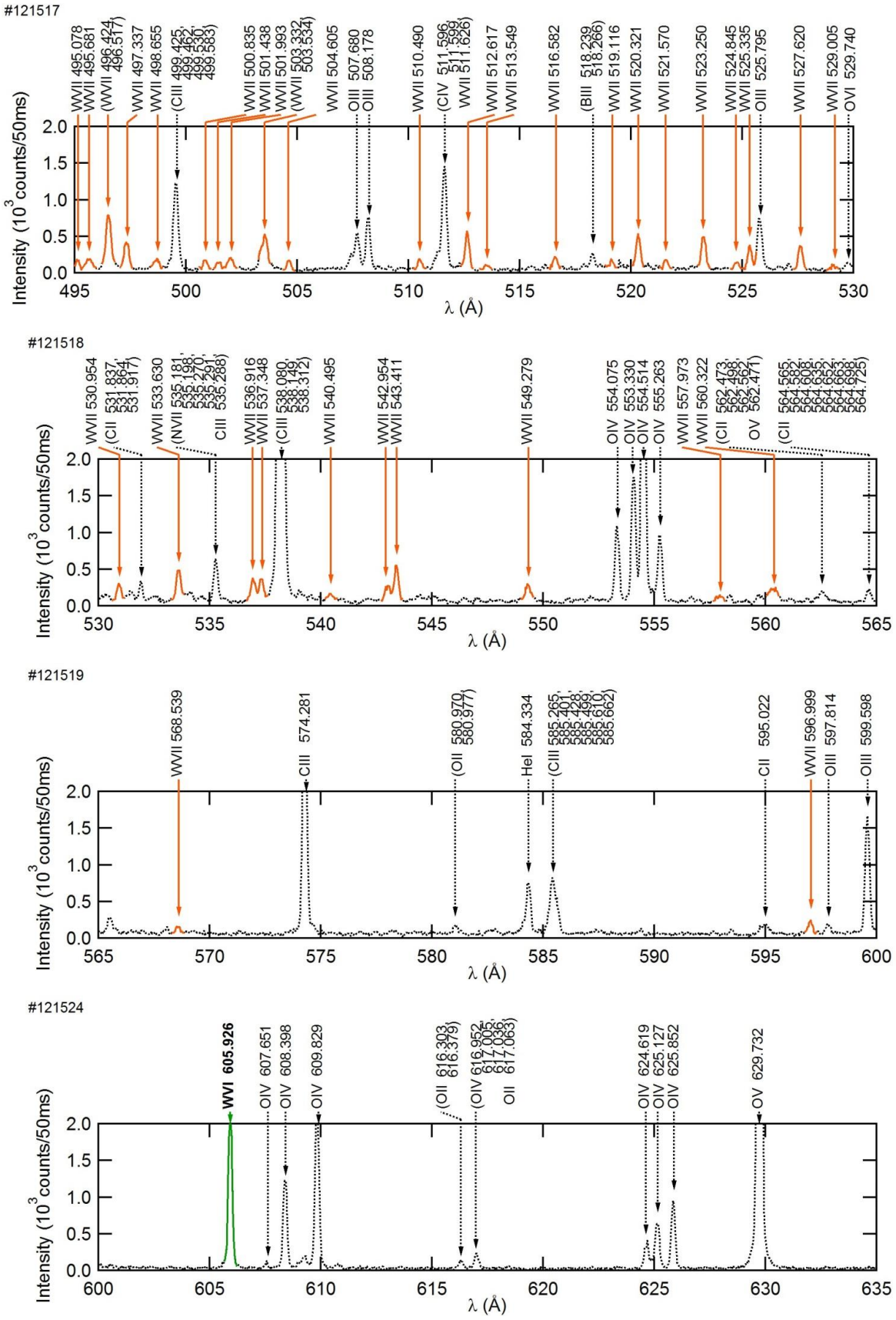

Figure 5 (a) VUV spectra of emission lines from W ions observed in LHD (495-635Å).

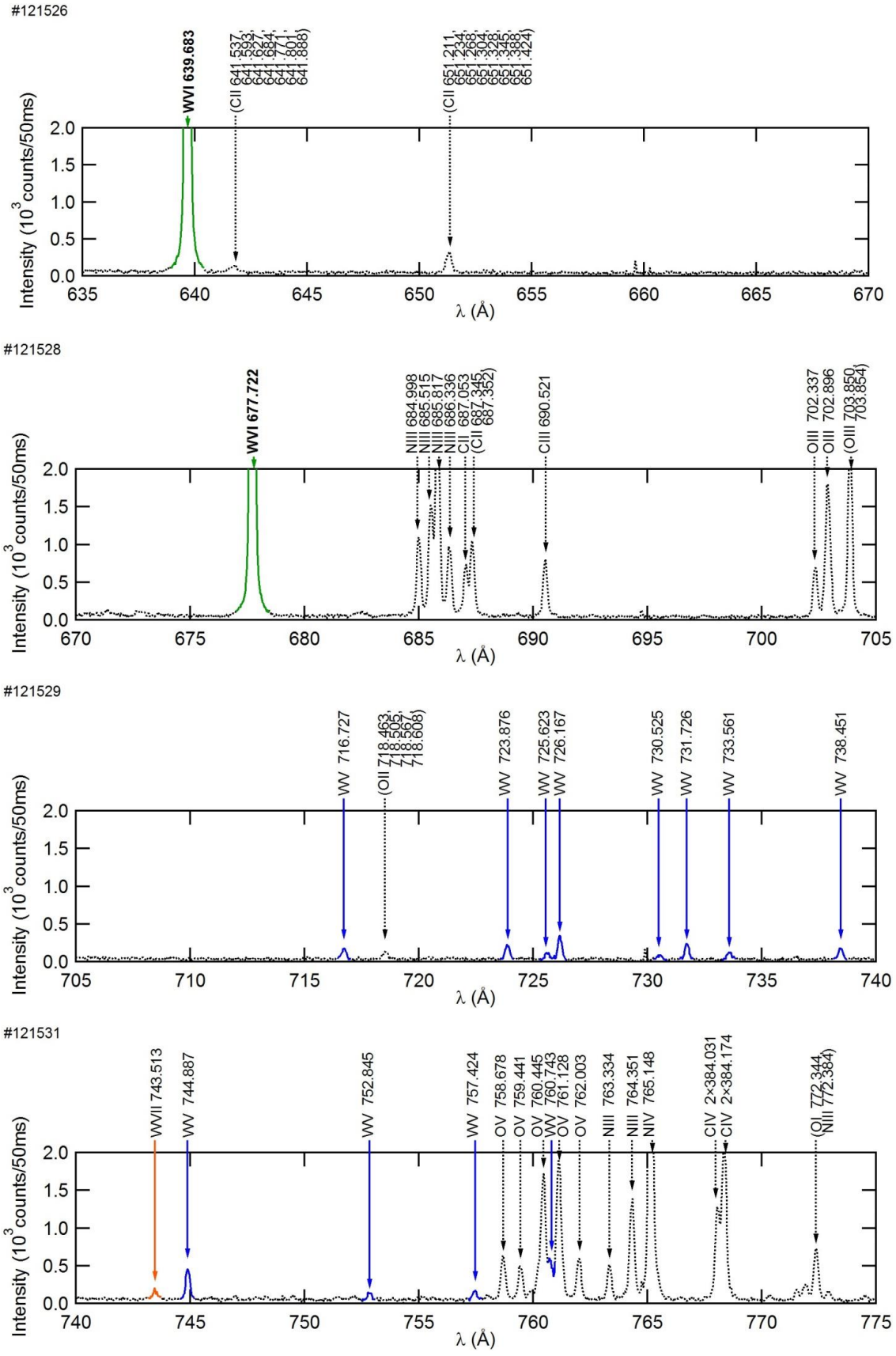

Figure 5 (b) (continued; 635-775Å)

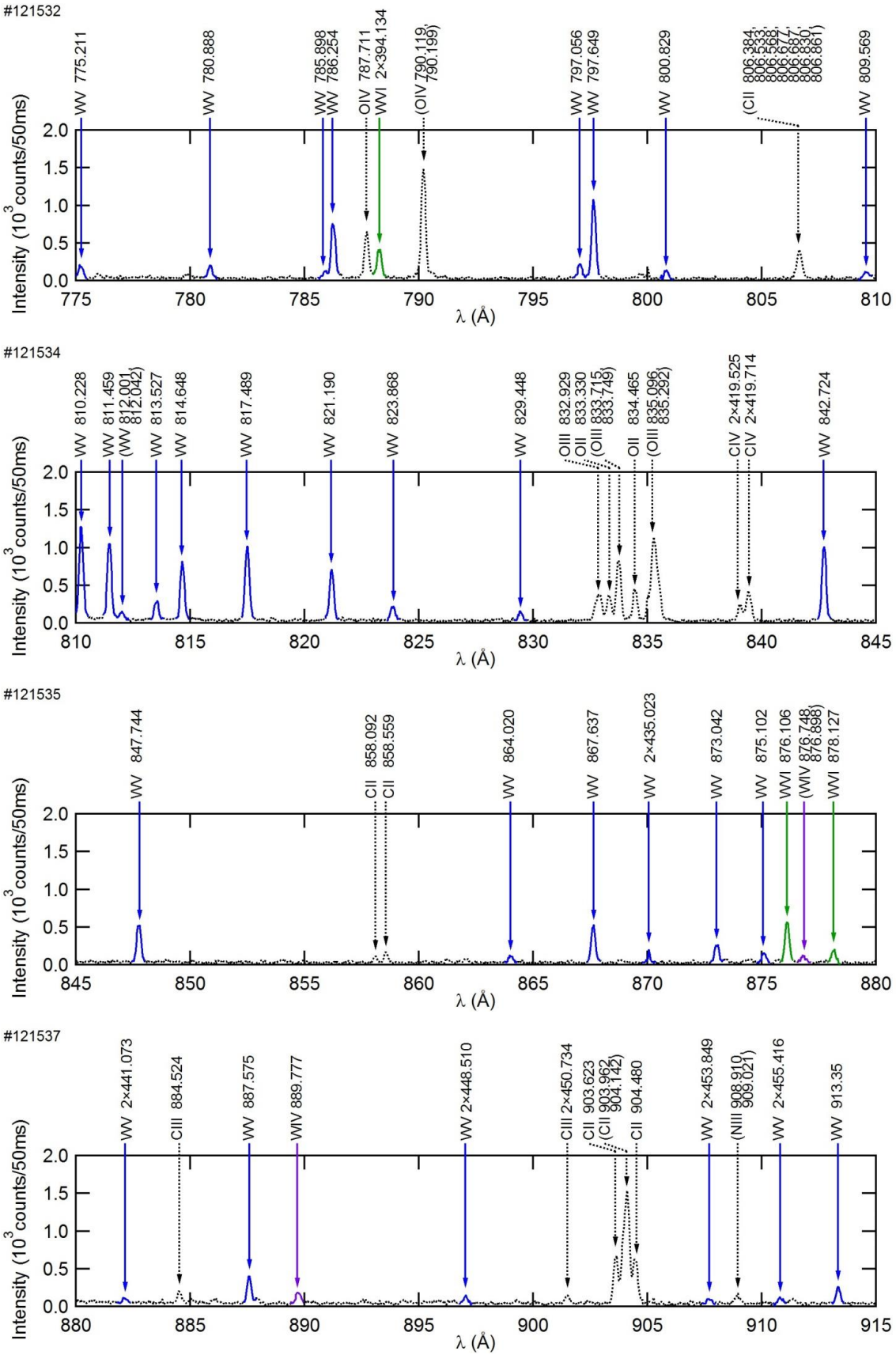

Figure 5 (c) (continued; 775-915Å)

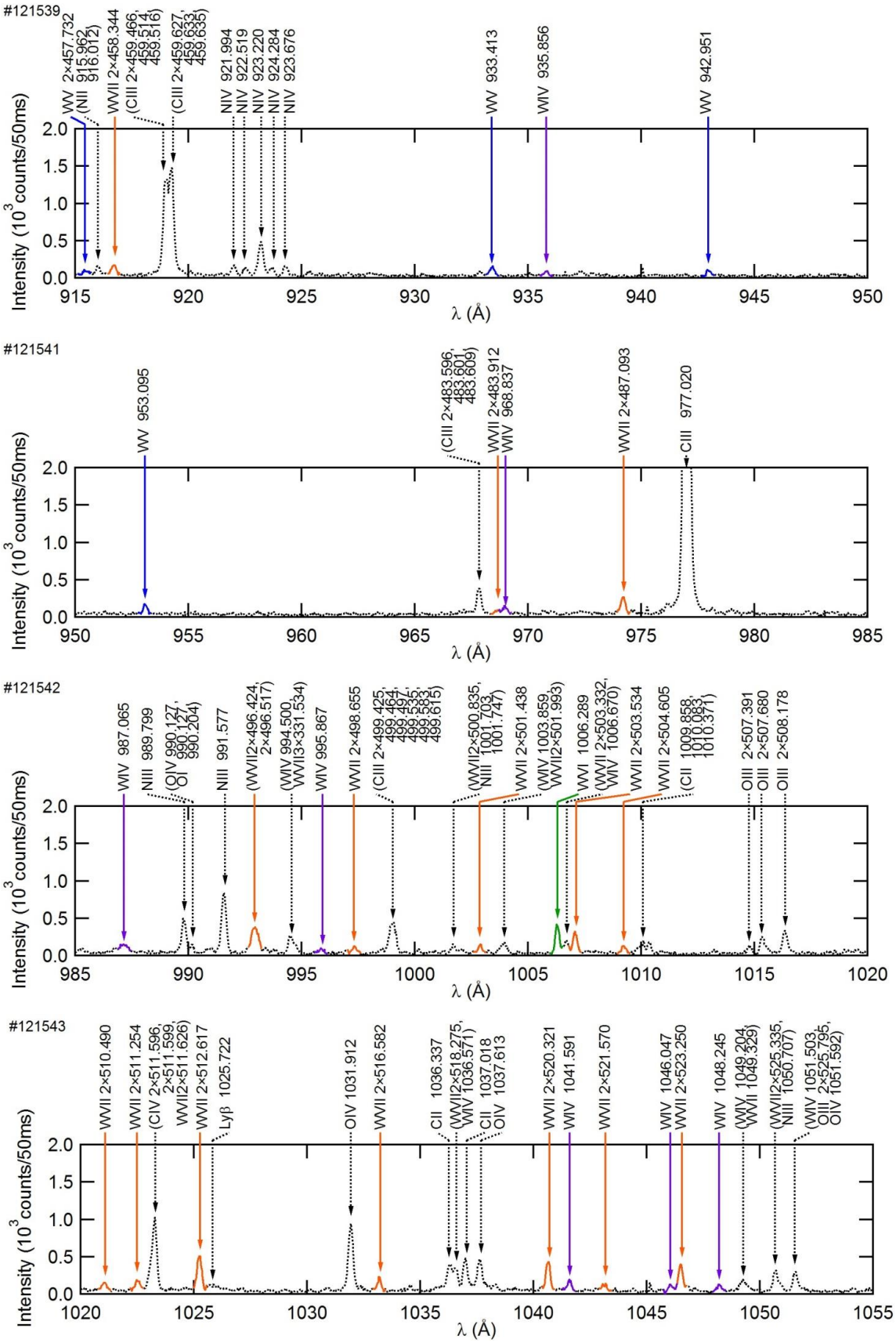

Figure 5 (d) (continued; 915-1055Å)

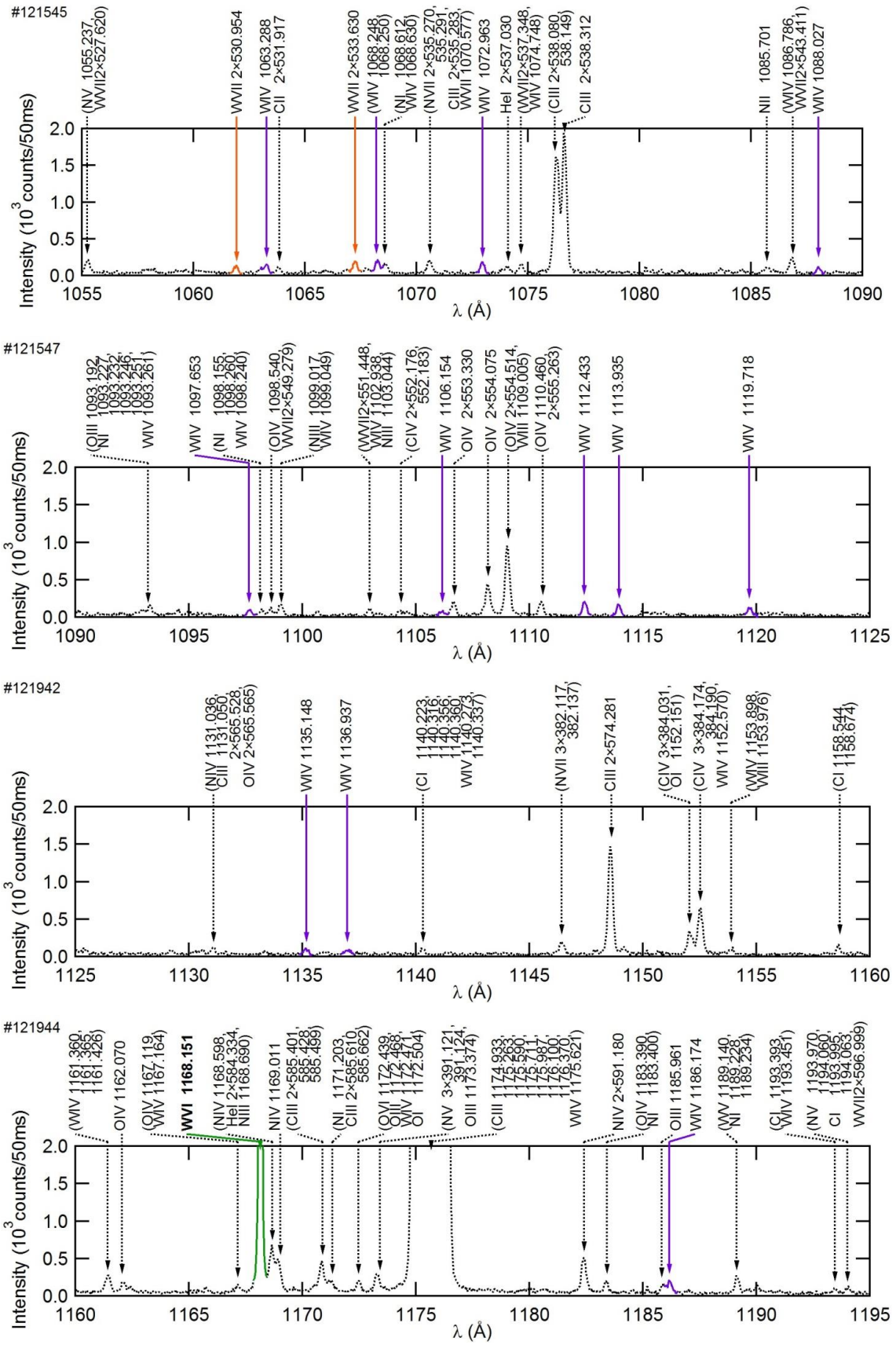

Figure 5 (e) (continued; 1055-1195Å)

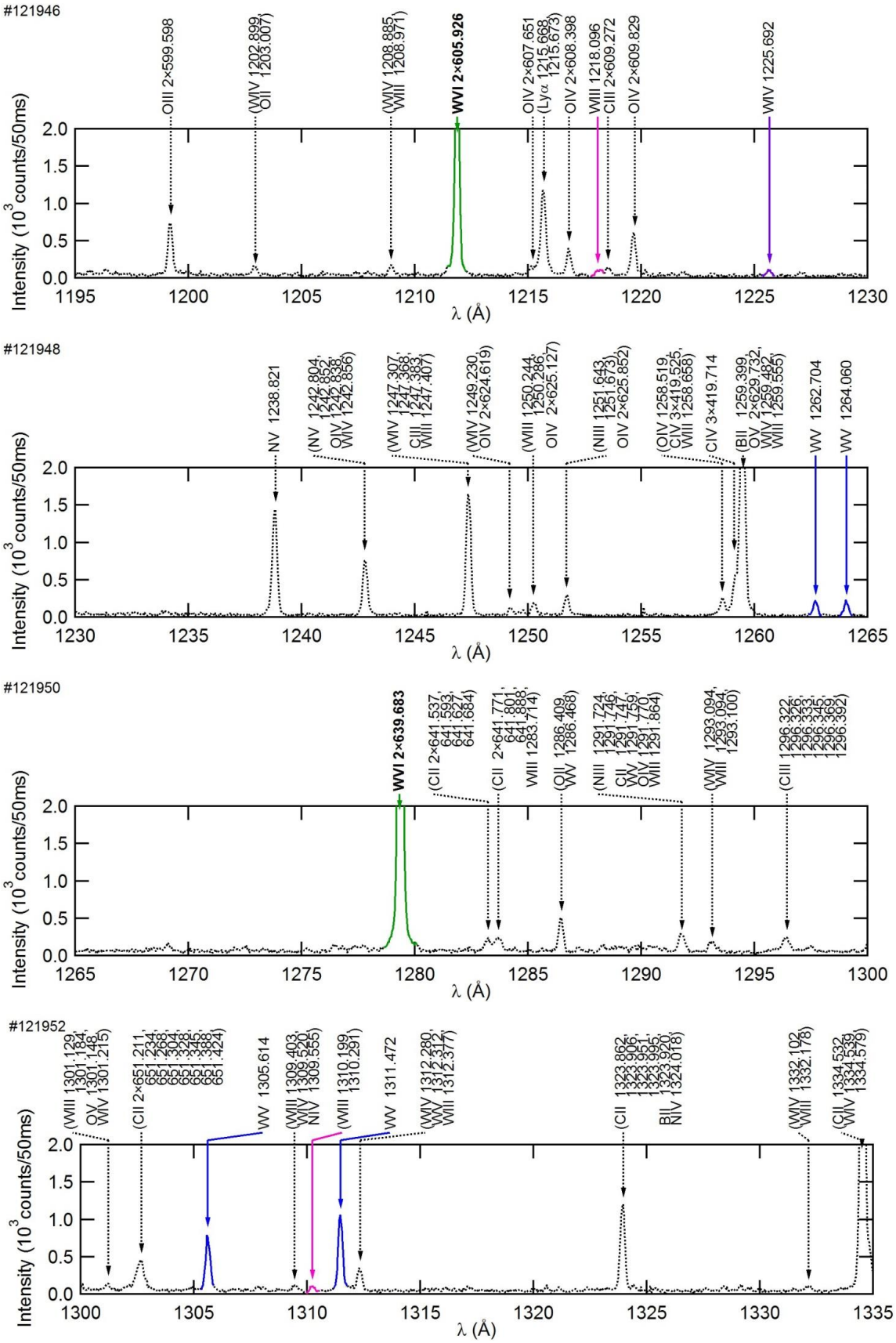

Figure 5 (f) (continued; 1195-1335Å)

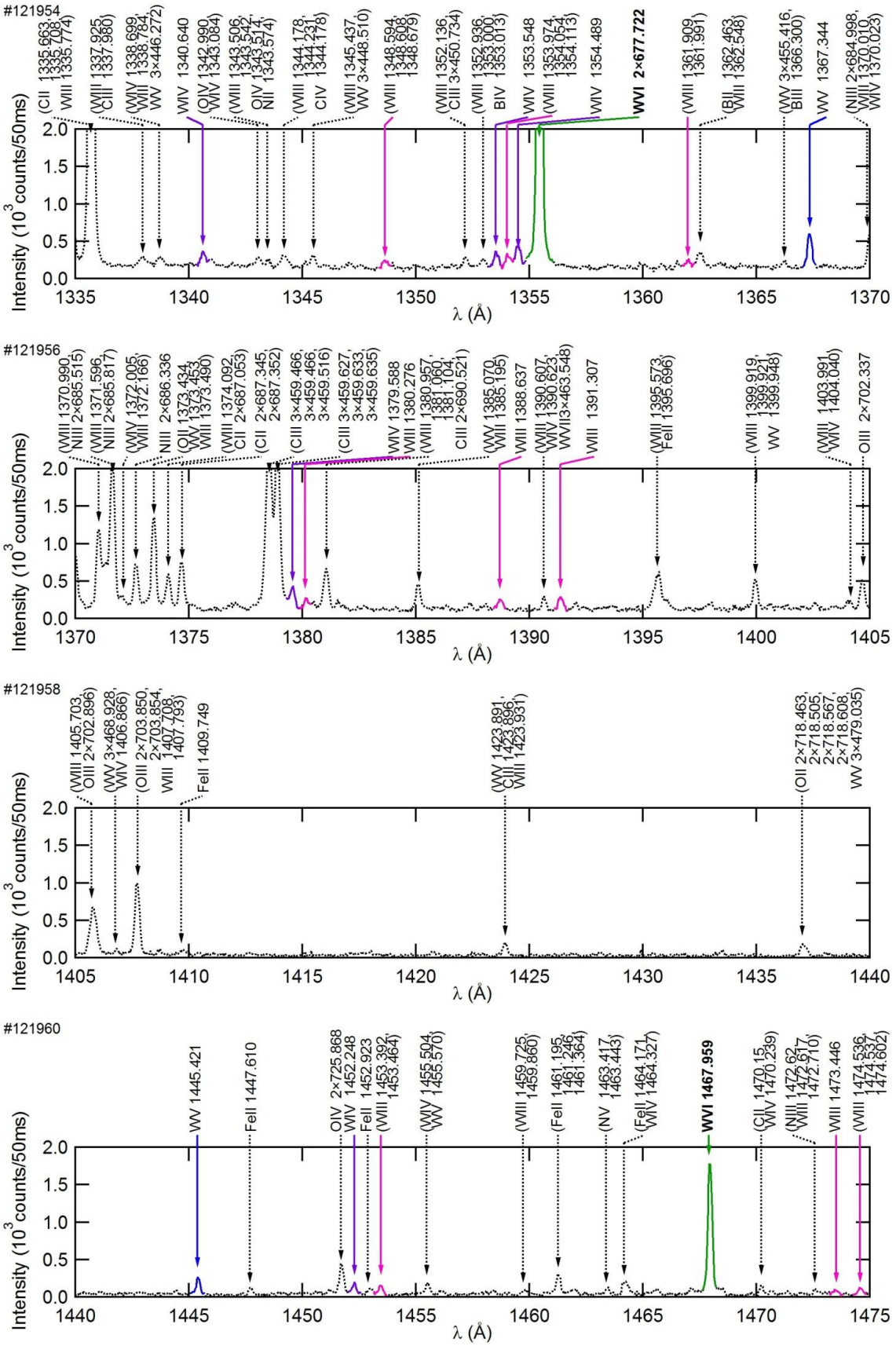

Figure 5 (g) (continued; 1335-1475Å)

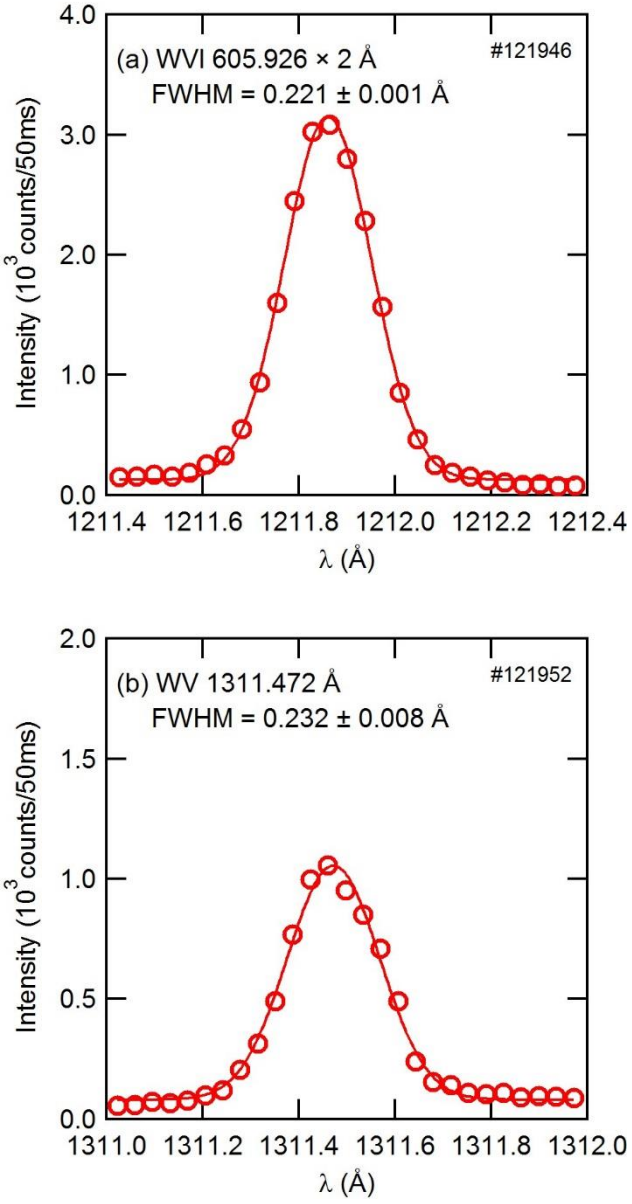

Figure 6　Spectral profiles of (a) 2 × W VI and (b) W V with Doppler broadening. Opened circles indicate raw experimental data and solid lines are fitting curves with Gaussian profiles.